Electronic Supplementary Material (ESI) for Inorganic Chemistry Frontiers.

Selective syntheses of homoleptic Ir(III) complexes bearing di-CF_3-functionalized benzoimidazol-2-ylidenes for generation of blue phosphorescence

Jie Yan,[a,‡] Yi Pan,[a,‡] I-Che Peng,[b,‡] Wen-Yi Hung,[b,*] Bingjie Hu,[a] Guowei Ni,[a] Shek-Man Yiu,[a] Yun Chi,[a,c,*] Kai Chung Lau,[a,*]

[‡] J.Y., Y.P. and I.P. contributed equally to this work.

(a) Department of Materials Science and Engineering and Department of Chemistry, City University of Hong Kong, Kowloon 999077, Hong Kong SAR, E-mail: yunchi@cityu.edu.hk and E-mail: kaichung@cityu.edu.hk

(b) Department of Optoelectronics and Materials Technology, Taiwan Ocean University, Keelung 20224, Taiwan, China, E-mail: wenhung@mail.ntou.edu.tw

(c) Center of Super-Diamond and Advanced Films (COSDAF), City University of Hong Kong, Kowloon 999077, Hong Kong SAR,

Keywords: (iridium, carbene, blue, organic light emitting diodes, cyclometalate)

Experimental section

General information and materials: Commercially available reagents were used without further purification. ^{1}H and ^{19}F NMR spectra were measured with a NMR 400MHz instrument (Bruker AVANCE III, BBO probe). Mass spectra were recorded on an Applied Biosystems 4800 Plus MALDI TOF/TOF Analyzer using 2,5-dihydroxybenzoic acid as the matrix substance. TGA measurements were performed on a TA Instrument TGAQ50, at a heating rate of 10 °C min^{-1} under a nitrogen atmosphere.

Photophysical measurements: UV-Vis spectra were measured with an UV-Visible NIR spectrophotometer system (HITACHI UH4150). The steady-state emission spectra were measured with a spectrofluorometer (Fluormax-4) and the lifetime decay spectra were measured with a photon-counting system (Edinburgh FLS980). All solution samples were degassed using at least three freeze-pump-thaw cycles. Photoluminescence quantum yields in solution are calculated using the standard sample which has a known quantum yield, while quantum yields in PMMA thin film was measured by an integrated sphere. Lifetimes were performed by an Edinburgh FLS980 time-correlated single photon counting (TCSPC) system with an EPL-375 diode laser as the excitation source.

Electrochemistry: Cyclic voltammetry was measured with an electrochemical analyzer (CHI660) equipped with a three-electrode system (glassy carbon: working electrode, platinum wire: auxiliary electrode, Ag/AgCl: reference electrode). Nitrogen-purged acetonitrile was used as solvent and NBu_4PF_6 (0.1 M) was used as supporting electrolyte. The potentials were referenced externally to the ferrocenium/ferrocene (Fc^+/Fc) couple.

2-Bromo-3,5-bis(trifluoromethyl)aniline (**A**)

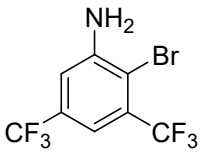

A solution of 3,5-bis(trifluoromethyl)aniline (11.46 g, 50 mmol) in 50 mL CH_2Cl_2 was cooled to 0 °C and a solution of *N*-bromosuccinimide (8.90 g, 50 mmol) in 350 mL of CH_2Cl_2 was slowly added at a temperature below 5 °C. The reaction was monitored by TLC. After

completed, the reaction mixture was washed with a saturated aqueous solution of $NaHCO_3$ (2 x 100 mL) and water (100 mL) in sequence. The organic phase was dried over Na_2SO_4 and the solvent was evaporated under reduced pressure. The crude product was purified by column chromatography on silica gel using petroleum ether/CH_2Cl_2 (4:1, v/v) as eluent to give off-white needles. Yield: 12.5 g (81.2%). ^{1}H NMR (400 MHz, $CDCl_3$) *δ* 7.28 (d, *J* = 2.0 Hz, 1H), 7.14 (d, *J* = 2.0 Hz, 1H), 4.62 (s, 2H); ^{19}F NMR (376 MHz, $CDCl_3$) δ –63.06 (s, 3F), –63.30 (s, 3F).

1-Phenyl-5,7-bis(trifluoromethyl)-1*H*-benzo[*d*]imidazole (**B1**)

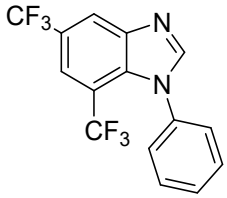

The mixture of **A** (3.08 g, 10 mmol), triethyl orthoformate (1.48 g, 1.66 mL, 10 mmol) and glacial acetic acid (30 mg, 29 μL, 0.5 mmol) was stirred at 120 °C for 4 h, then cooled to RT. Aniline (0.93 g, 0.91 mL, 10 mmol) was added and the resulting mixture was stirred at 140 °C for 12 h. After cooled to RT, DBU (1.52 g, 1.5 mL, 10 mmol), CuI (190 mg, 1.0 mmol) and DMSO (20 mL) were added, and the reaction mixture was stirred overnight at 150 °C. After then, ethyl acetate (50 mL) was added and, the mixture was filtered through a Celite pad. The filtrate was washed with brine and water in sequence, dried over anhydrous Na_2SO_4 and concentrated by rotatory evaporation. The crude product was purified by column chromatography using petroleum ether/ethyl acetate (4/1, v/v) as eluent to give a white solid. Yield: 1.49 g (45.2%). ^{1}H NMR (400 MHz, $CDCl_3$) δ 8.36 (s, 1H), 8.09 (s, 1H), 7.87 (s, 1H), 7.62-7.53 (m, 3H), 7.42 (d, *J* = 6.4 Hz, 2H); ^{19}F NMR (376 MHz, $CDCl_3$) δ –57.30 (s, 3F), –61.15 (s, 3F).

1-(4-(*tert*-Butyl)phenyl)-5,7-bis(trifluoromethyl)-1*H*-benzo[*d*]imidazole (**B2**)

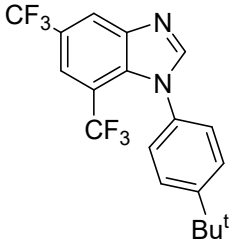

This compound was prepared similarly as **B1**, giving an off-white solid. Yield: 1.60 g (41.5%). ^{1}H NMR (400 MHz, $CDCl_3$) δ 8.35 (s, 1H), 8.07 (s, 1H), 7.86 (s, 1H), 7.54 (d, *J* = 8.4 Hz, 2H), 7.30 (d, *J* = 8.4 Hz, 2H), 1.40 (s, 9H); ^{19}F NMR (376 MHz, $CDCl_3$, 296 K): δ –57.31 (s, 3F), –61.13 (s, 3F)

3-Methyl-1-phenyl-5,7-bis(trifluoromethyl)-1*H*-benzo[*d*]imidazol-3-ium trifluoromethanesulfonate (**C1**)

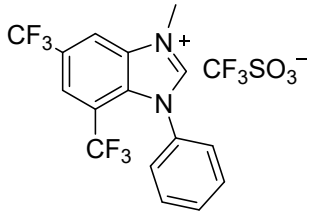

Compound **B1** (1.16 g, 3.5 mmol) was dissolved in toluene (40 mL) and, methyl trifluoromethanesulfonate (1.72 g, 1.19 mL, 10.5 mmol) was added dropwise and the reaction mixture was stirred for 4 h at RT. The resulting precipitate was filtered off, washed with toluene, and dried overnight under vacuum to provide a colorless solid. Yield: 1.65 g (95.1%). ^{1}H NMR (400 MHz, DMSO-d_6) δ 10.35 (s, 1H), 9.15 (s, 1H), 8.43 (s, 1H), 7.79 – 7.66 (m, 5H), 4.28 (s, 3H); ^{19}F NMR (376 MHz, DMSO-d_6) δ –55.72 (s, 3F), –59.94 (s, 3F), –77.81 (s, 3F).

1-(4-(*tert*-Butyl)phenyl)-3-methyl-5,7-bis(trifluoromethyl)-1*H*-benzo[*d*]imidazol-3-ium trifluoromethanesulfonate (**C2**)

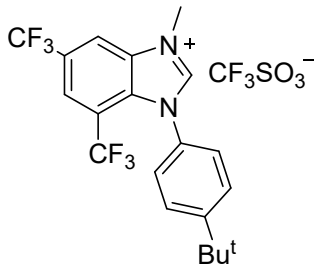

This compound was prepared similarly to **C1**, giving a white powder. Yield: 1.78 g (92.3%). ^{1}H NMR (400 MHz, DMSO-d_6) δ 10.32 (s, 1H), 9.13 (s, 1H), 8.41 (s, 1H), 7.60 (d, *J* = 8.5 Hz, 2H), 7.49 (d, *J* = 8.5 Hz, 2H), 4.26 (s, 3H), 1.36 (s, 9H); ^{19}F NMR (376 MHz, DMSO-d_6) δ –55.75 (s, 3F), –59.94 (s, 3F), –77.81 (s, 3F).

3-(4-(*tert*-Butyl)phenyl)-1-phenyl-5,7-bis(trifluoromethyl)-1*H*-benzo[d]imidazol-3-ium trifluoromethanesulfonate (**C3**).

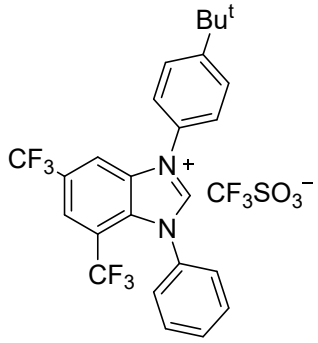

To a 50 mL round-bottom flask was added **B1** (500 mg, 1.5 mmol), $Cu(OAc)_2 \cdot H_2O$ (14 mg, 0.07 mmol), bis(4-*tert*-butylphenyl)iodonium trifluoromethanesulfonate (990 mg, 1.8 mmol) and 20 mL DMF. After stirred at 110 °C for 12 hours, the solvent was concentrated to half under reduced pressure, followed by addition of deionized water to induce precipitation. The precipitate was collected and washed with deionized water and methanol in sequence, and dried under vacuum to attain an off-white powder 734 mg (80%). ^{1}H NMR (400 MHz, $CDCl_3$, 296 K): δ 9.21 (s, 1H), 8.25 (s, 1H), 8.20 (s, 1H), 7.79 (d, *J* = 8.0 Hz, 2H), 7.65 – 7.61 (m, 5H), 7.16 (d, *J* = 8.0 Hz, 2H), 1.31 (s, 9H); ^{19}F NMR (376 MHz, $CDCl_3$, 296 K): δ –56.89 (s, 3F), –61.90 (s, 3F), –78.66 (s, 3F).

1-(4-(*tert*-Butyl)phenyl)-3-phenyl-5,7-bis(trifluoromethyl)-1*H*-benzo[d]imidazol-3-ium trifluoromethanesulfonate (**C4**).

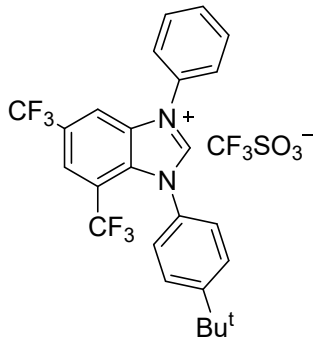

This compound was prepared from **B2** and diphenyliodonium trifluoromethane-sulfonate. Yield: 400 mg (83%). ^{1}H NMR (400 MHz, $CDCl_3$, 296 K): δ 9.60 (s, 1H), 8.20 (s, 1H),

8.12 (s, 1H), 7.88 (d, *J* = 8.4 Hz, 2H), 7.72 – 7.68 (m, 5H), 7.59 (d, *J* = 8.4 Hz, 2H), 1.38 (s, 9H). ^{19}F NMR (376 MHz, $CDCl_3$, 296 K): δ –56.89 (s, 3F), –61.96 (s, 3F), –78.68 (s, 3F).

Computational details of theoretical investigations: The geometries, electronic structures, and electronic excitations of the studied Ir(III) complexes were investigated at the B3LYP-D3(BJ)/def2-SVP level[1] with Gaussian 16 set of programs.[2] The solvent effect of toluene was taken account by the polarizable continuum model (PCM).[3] The corresponding ground state (S_0) and lowest triplet state (T_1) geometries were optimized based on the X-ray structural data of ***m*-Ir(dfp)$_3$** and ***f*-Ir(tBpp)$_3$**. A total of 10 low-lying excited states ($T_1 \sim T_5$ and $S_1 \sim S_5$) were included in the TD–DFT calculation[4] based on the optimized S_0 structure. Natural transition orbital (NTO) analysis[5] was applied to obtain a clear and compact orbital representation for the electronic excitation described by a variety of orbital transitions without a single predominant one (e.g. $S_0 \rightarrow T_1$ excitation in this work) at optimized S_0 structure. The IFCT (interfragment charge transfer) method analysis in the $S_0 \rightarrow T_1$ excitation is using Multiwfn software.[6] The Hirshfeld method is used to calculate the density in IFCT analysis.[7]

The spin-orbit coupling (SOC)-TDDFT calculation[8] was performed using B3LYP functional with ZORA Hamiltonian[9] (SARC-ZORA-SVP for Ir and ZORA-def2-SVP for other elements) at the optimized S_0 and T_1 structures in ORCA (v5.0.3) software.[10] A total of 100 low-lying excited states (50 for singlet and 50 for triplet) were included in the SOC-TDDFT calculation in toluene with COSMO model.[11] The radiative lifetime (τ_{rad}) and radiative rate (k_r) are calculated by the arithmetic average and Boltzmann average (at 298 K) of the SOC substates of T_1.[8]

Device fabrication and measurement: All chemicals were purified by vacuum sublimation before the fabrications. The OLED were fabricated through vacuum deposition of the materials at 10^{-6} torr onto the ITO coated glass substrates possessing a sheet resistance of 15 Ω sq^{-1}. The ITO surface was cleaned ultrasonically, i.e., with acetone, methanol, and

deionized water in sequence and finally with N_2 plasma. The deposition rate of each organic material was ca. 1 – 2 Å·s^{-1}. The J–V–L characteristics of the devices were measured in a glovebox at the same time. For device characterization, the driving source was supplied from the programmable source measurement unit (2614B, Keithley) while the light intensity was measured by a calibrated silicon detector. EL spectra were recorded using a photodiode array (Ocean Optics USB2000+).

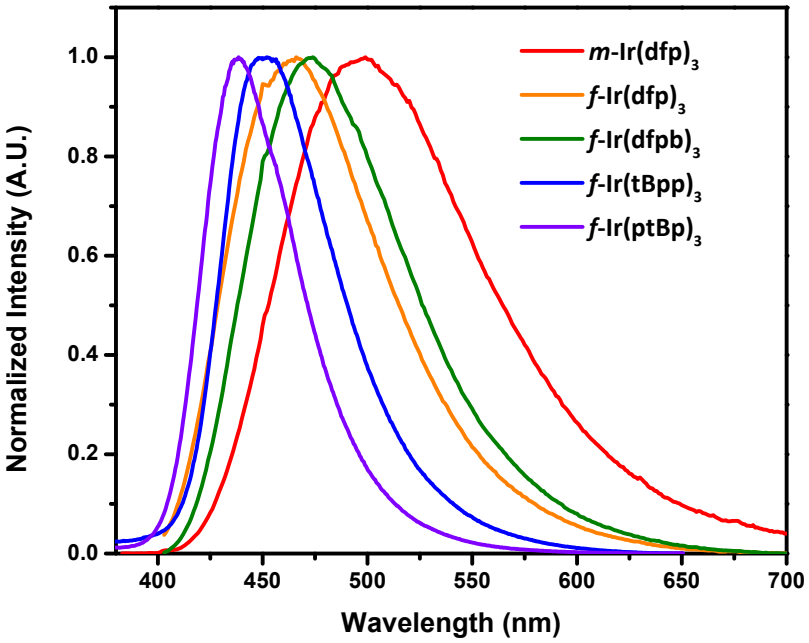

Figure S1. Emission of the studied Ir(III) carbene complexes in PMMA thin films at 2 wt.% at RT.

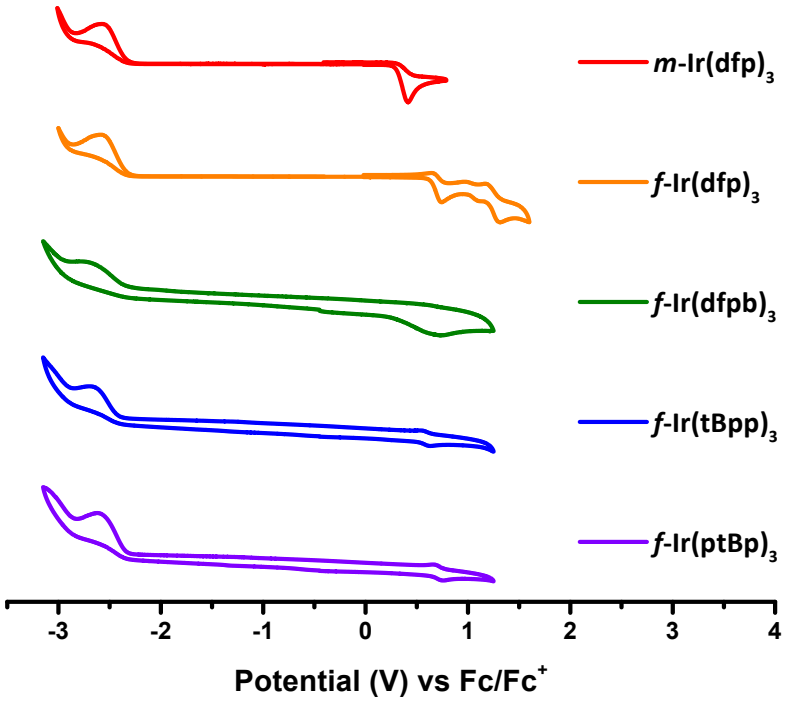

Figure S2. Cyclic voltammograms of studied tris-bidentate Ir(III) complexes in acetonitrile

solution.

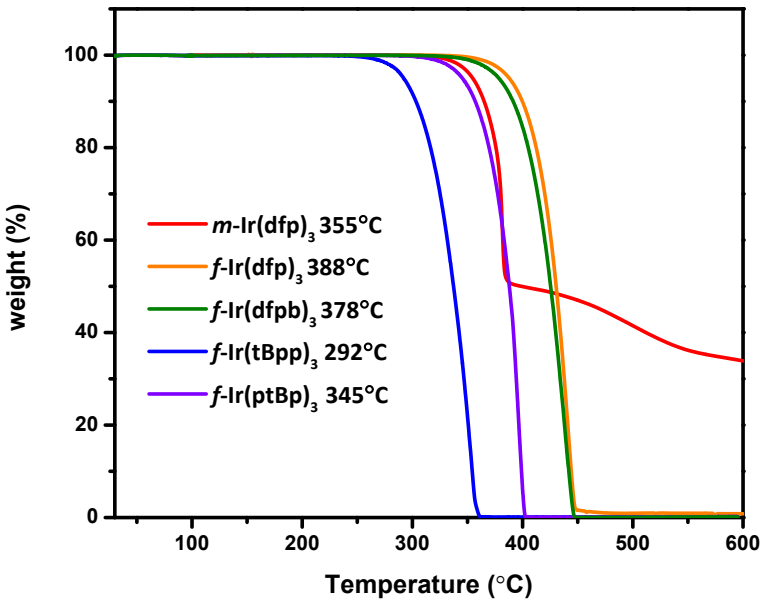

Figure S3. TGA data of studied Ir(III) complexes with decomposition temperature (T_d) at a weight loss of 5 wt.%.

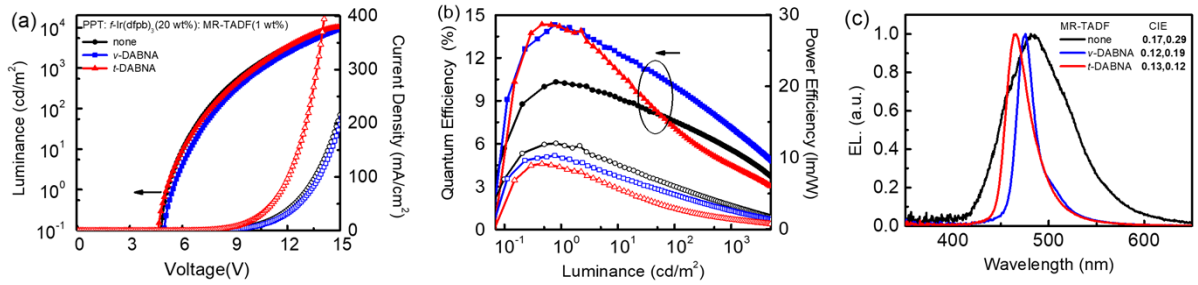

Figure S4. (a) current density–voltage–luminance (J–V–L) characteristics, (b) EQE and PE as a function of luminance, and (c) EL spectra using ***f*-Ir(dfpb)$_3$** as a sensitizer.

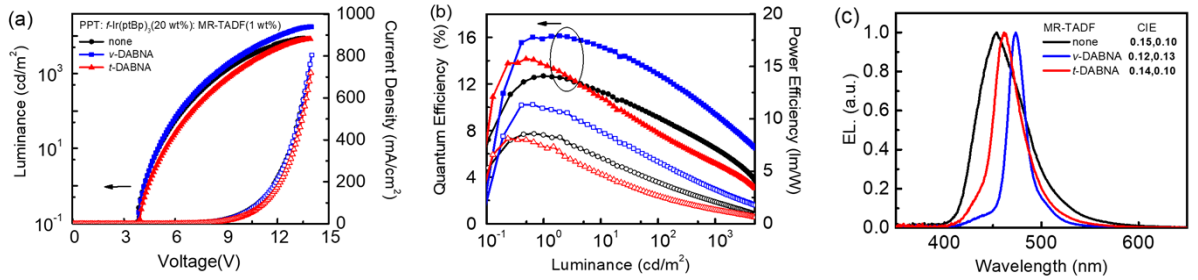

Figure S5. (a) current density–voltage–luminance (J–V–L) characteristics, (b) EQE and PE as a function of luminance, and (c) EL spectra using ***f*-Ir(ptBp)$_3$** as a sensitizer.

Table S1. Summarized electrochemical data, energy gap and decomposition temperature of the studied Ir(III) complexes.

complexes	**E_{ox}^{onset} [a]**	**E_{pc}^{re} (V) [b]**	**HOMO (eV) [c]**	**energy gap (eV) [d]**	**LUMO (eV) [e]**	**T_d, 5% (°C) [f]**
***m*-Ir(dfp)$_3$**	0.30	–2.33	–5.10	2.64	–2.46	355
***f*-Ir(dfp)$_3$**	0.64	–2.33	–5.44	2.96	–2.48	388
***f*-Ir(dfpb)$_3$**	0.58	–2.39	–5.38	2.94	–2.44	378
***f*-Ir(tBpp)$_3$**	0.52	–2.44	–5.32	3.00	–2.32	292
***f*-Ir(ptBp)$_3$**	0.64	–2.35	–5.44	3.07	–2.37	345

[a] All electrochemical potentials were measured in a 0.1 M acetonitrile solution of $TBAPF_6$ referenced to the Fc/Fc^+ couple; E_{ox}^{onset} is the anodic wave potential for the oxidation wave; *[b]* E_{pc}^{re} is the cathodic wave potential for the irreversible reduction wave; *[c]* HOMO = $-(E^{ox}_{½} + 4.8)$; *[d]* energy gap = 1240 / [PL_{onset} (nm)]; *[e]* LUMO = HOMO + energy gap; *[f]* TGA is recorded under N_2 flow.

Table S2. The blend-film PLQYs of v-DABNA and t-DABNA in the Ir(III) complexes and PPT

Sample	excited λ_{max} (nm)	em λ_{max} (nm)	Φ (%)
PPT:***f*-Ir(dfpb)$_3$**(20 wt%)	330	469	73.4
PPT:***f*-Ir(dfpb)$_3$**(20 wt%):v-DABNA(1 wt%)	330	474	89
PPT:***f*-Ir(dfpb)$_3$**(20 wt%):t-DABNA(1 wt%)	330	462	80.8
PPT:***f*-Ir(tBpp)$_3$**(20 wt%)	330	458	90.8
PPT:***f*-Ir(tBpp)$_3$**(20 wt%):v-DABNA(1 wt%)	330	474	97
PPT:***f*-Ir(tBpp)$_3$**(20 wt%):t-DABNA(1 wt%)	330	458	93.8
PPT:***f*-Ir(ptBp)$_3$**(20 wt%)	330	448	73.6
PPT:***f*-Ir(ptBp)$_3$**(20 wt%):v-DABNA(1 wt%)	330	474	88
PPT:***f*-Ir(ptBp)$_3$**(20 wt%):t-DABNA(1 wt%)	330	462	81.6

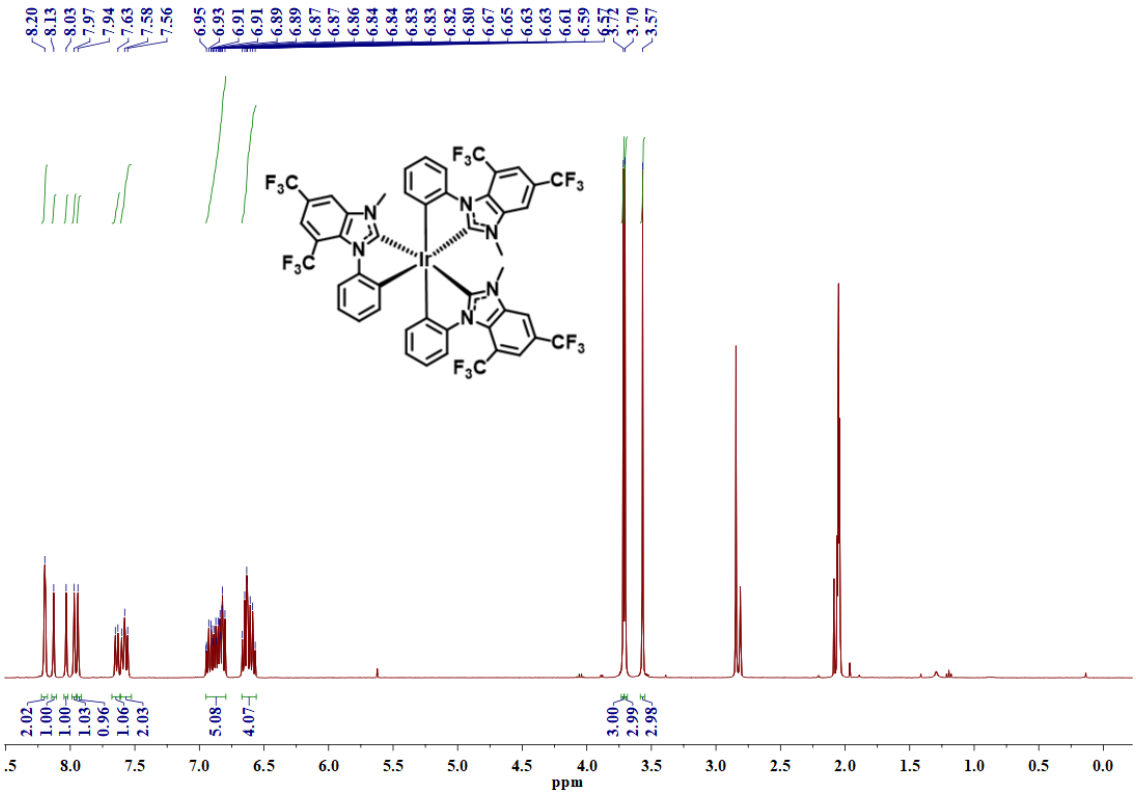

Figure S6. ^{1}H NMR (400 MHz) spectrum of ***m*-Ir(dfp)$_3$** recorded in acetone-d_6 solution at RT.

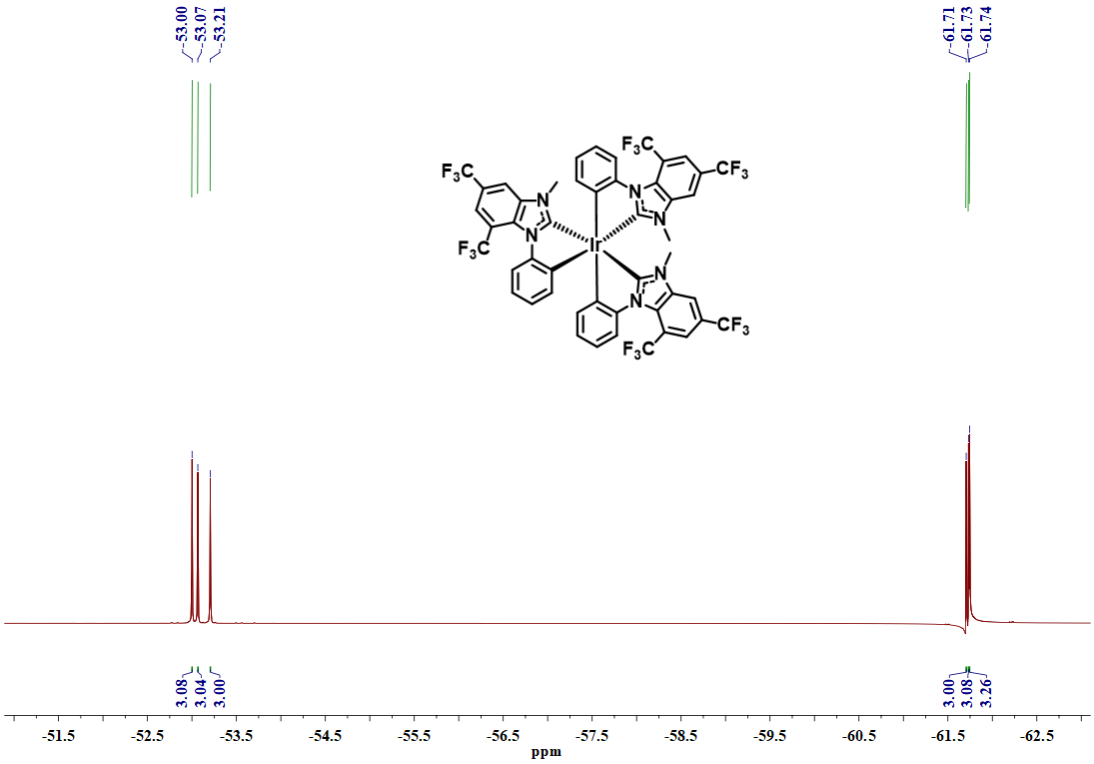

Figure S7. ^{19}F NMR (376 MHz) spectrum of ***m*-Ir(dfp)$_3$** recorded in acetone-d_6 solution at RT.

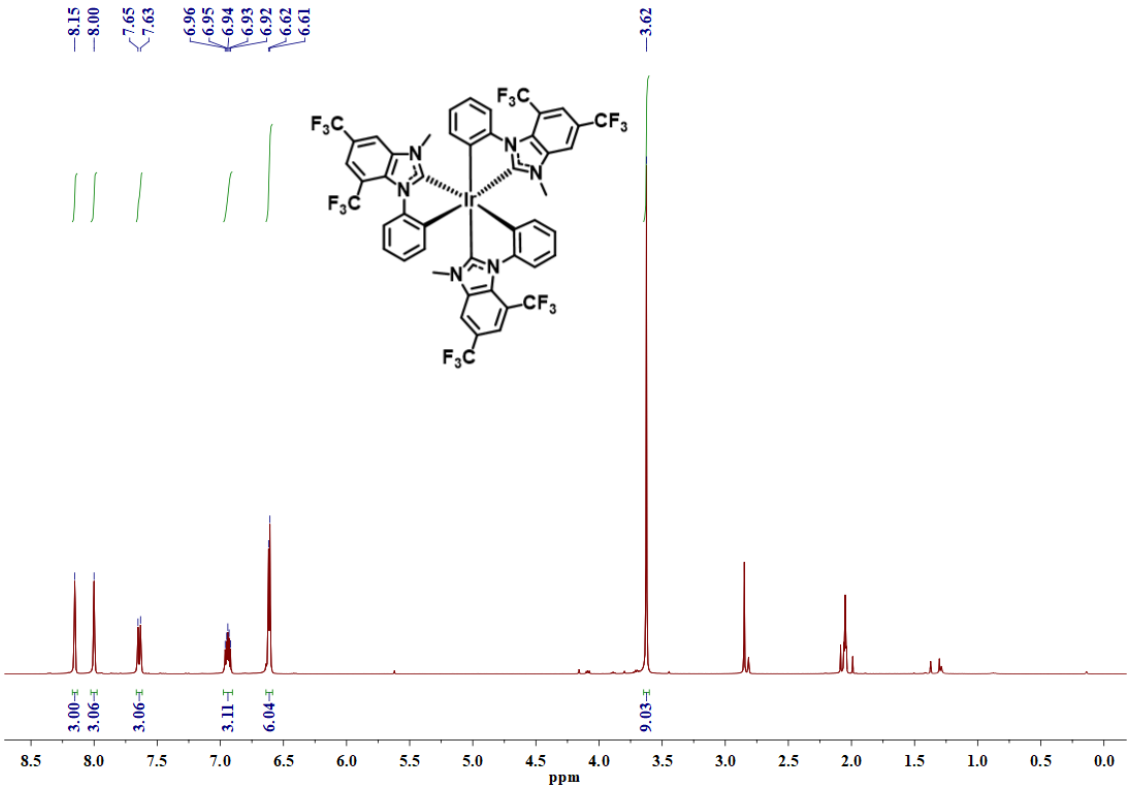

Figure S8. ^{1}H NMR (400 MHz) spectrum of ***f*-Ir(dfp)$_3$** recorded in acetone-d_6 solution at RT.

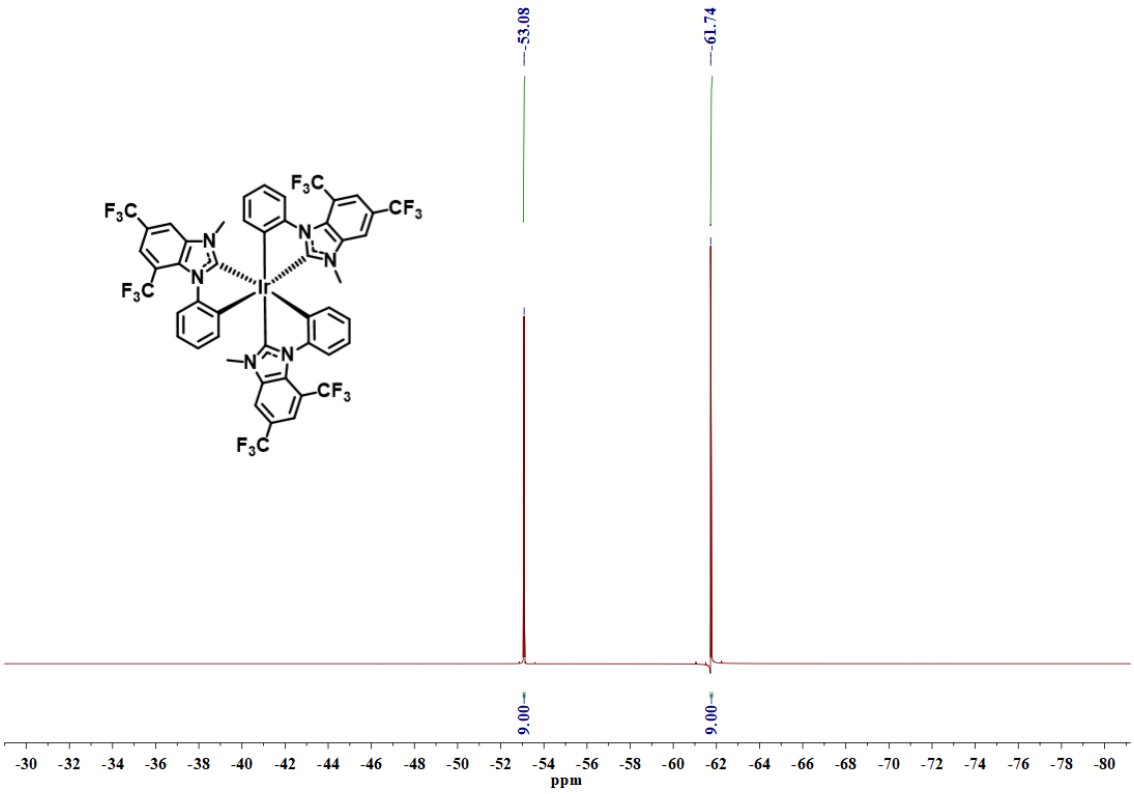

Figure S9. ^{19}F NMR (376 MHz) spectrum of ***f*-Ir(dfp)$_3$** recorded in acetone-d_6 solution at RT.

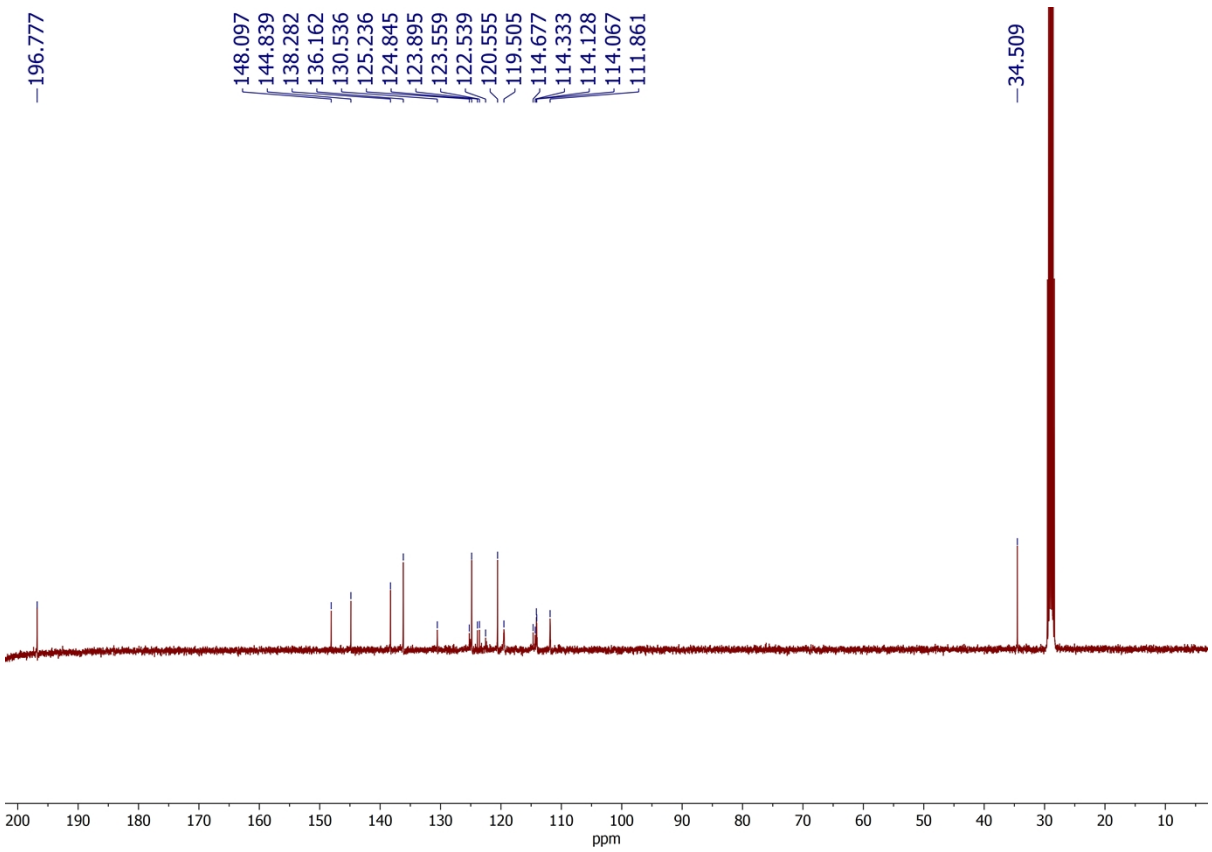

Figure S10. ^{13}C NMR (100 MHz) spectrum of ***f*-Ir(dfp)$_3$** recorded in acetone-d_6 solution at RT.

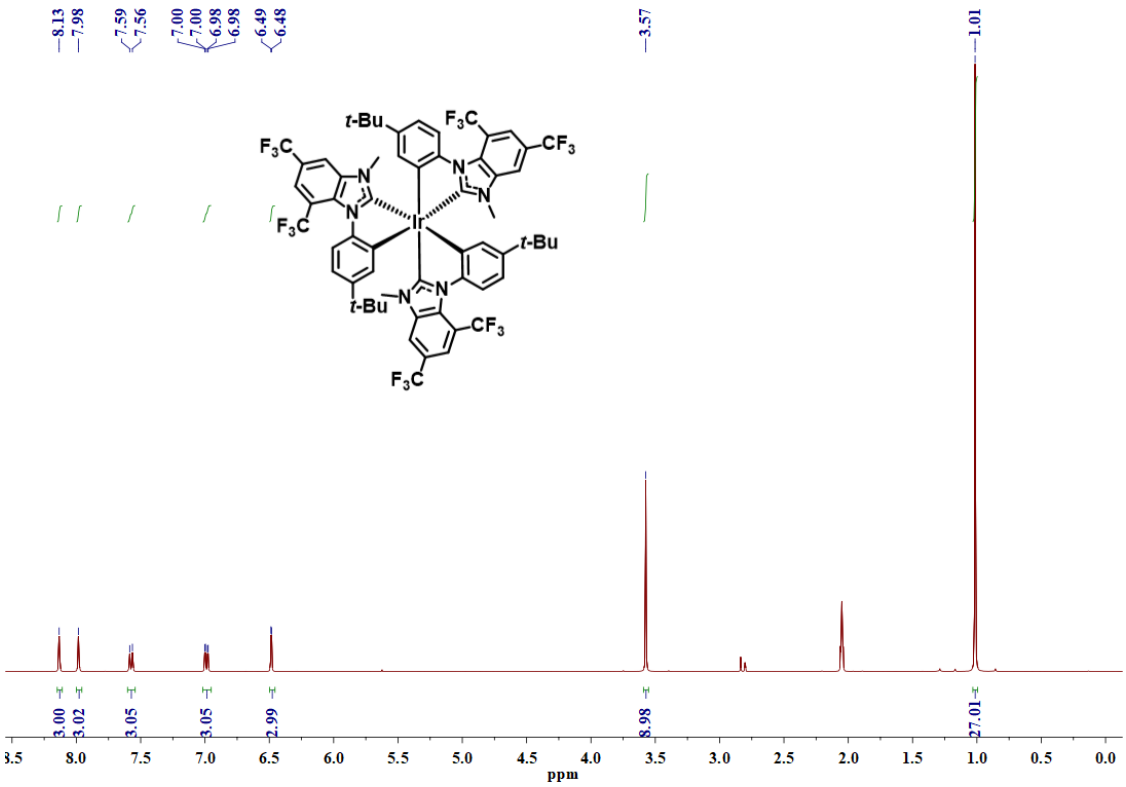

Figure S11. ^{1}H NMR (400 MHz) spectrum of ***f*-Ir(dfpb)$_3$** recorded in acetone-d_6 solution at RT.

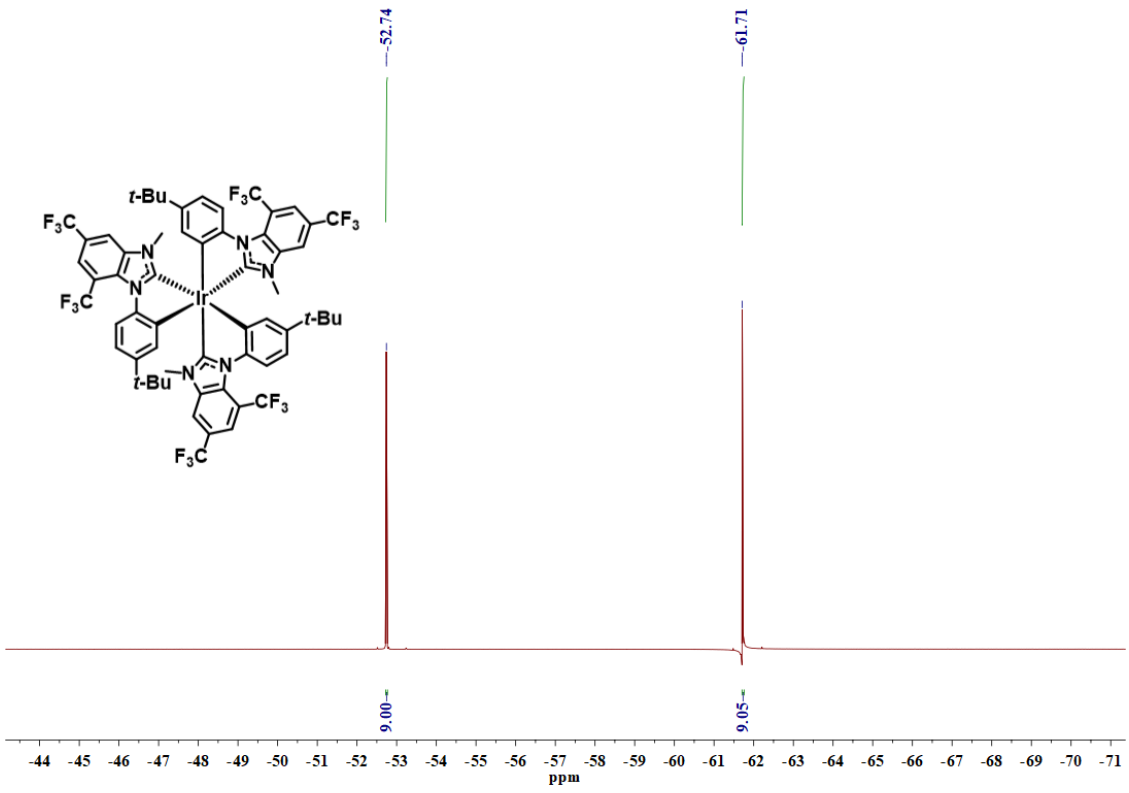

Figure S12. ^{19}F NMR (376 MHz) spectrum of ***f*-Ir(dfpb)$_3$** recorded in acetone-d_6 solution at RT.

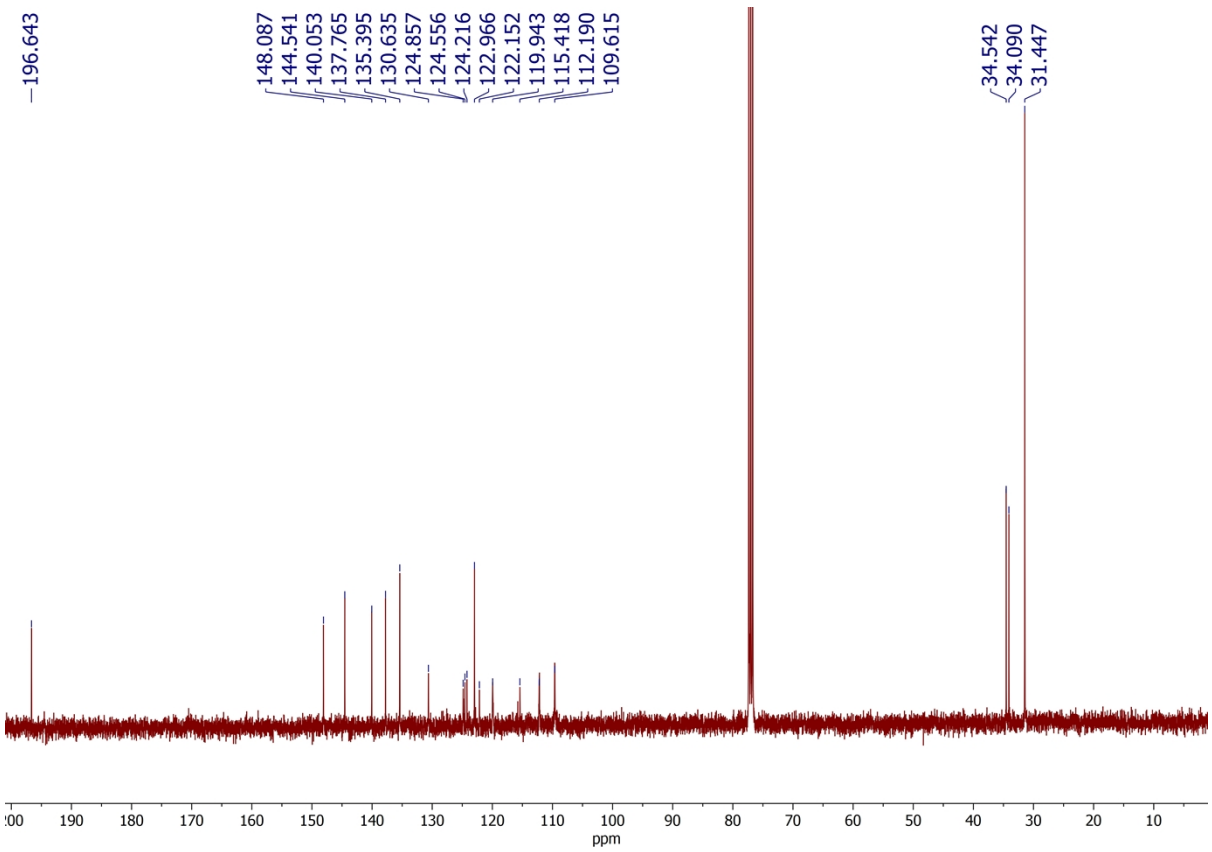

Figure S13. ^{13}C NMR (100 MHz) spectrum of ***f*-Ir(dfpb)$_3$** recorded in $CDCl_3$ solution at RT.

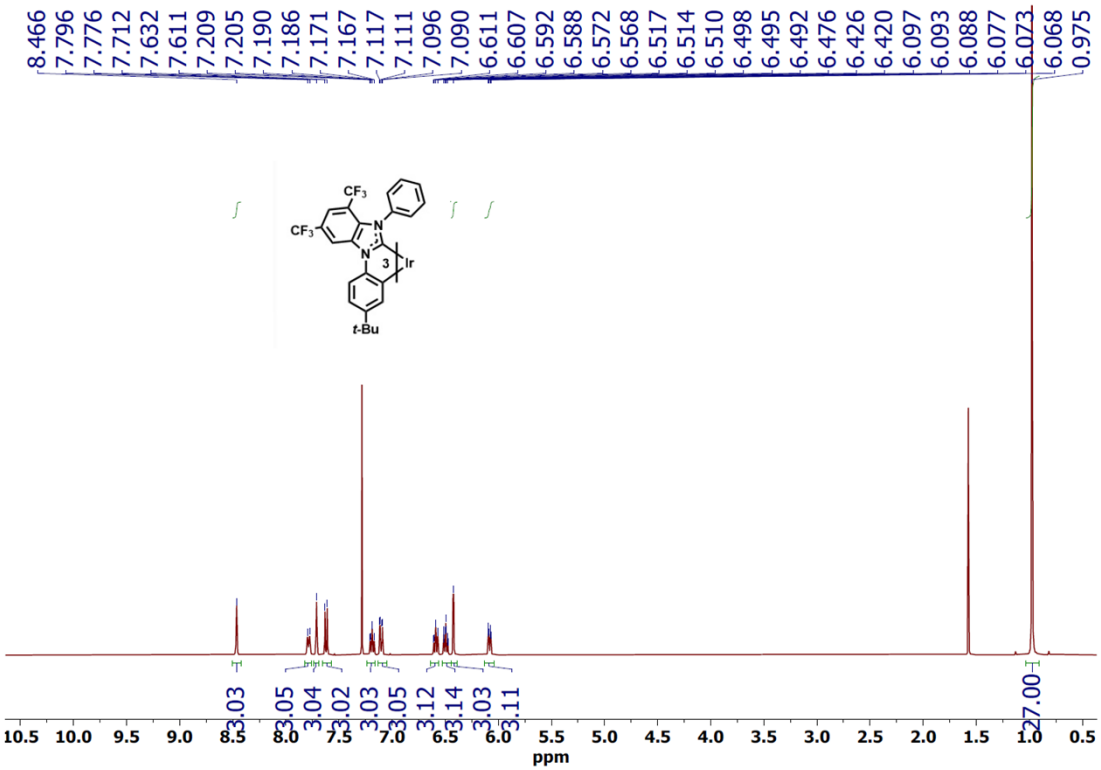

Figure S14. ^{1}H NMR (400 MHz) spectrum of ***f*-Ir(tBpp)$_3$** recorded in $CDCl_3$ solution at RT.

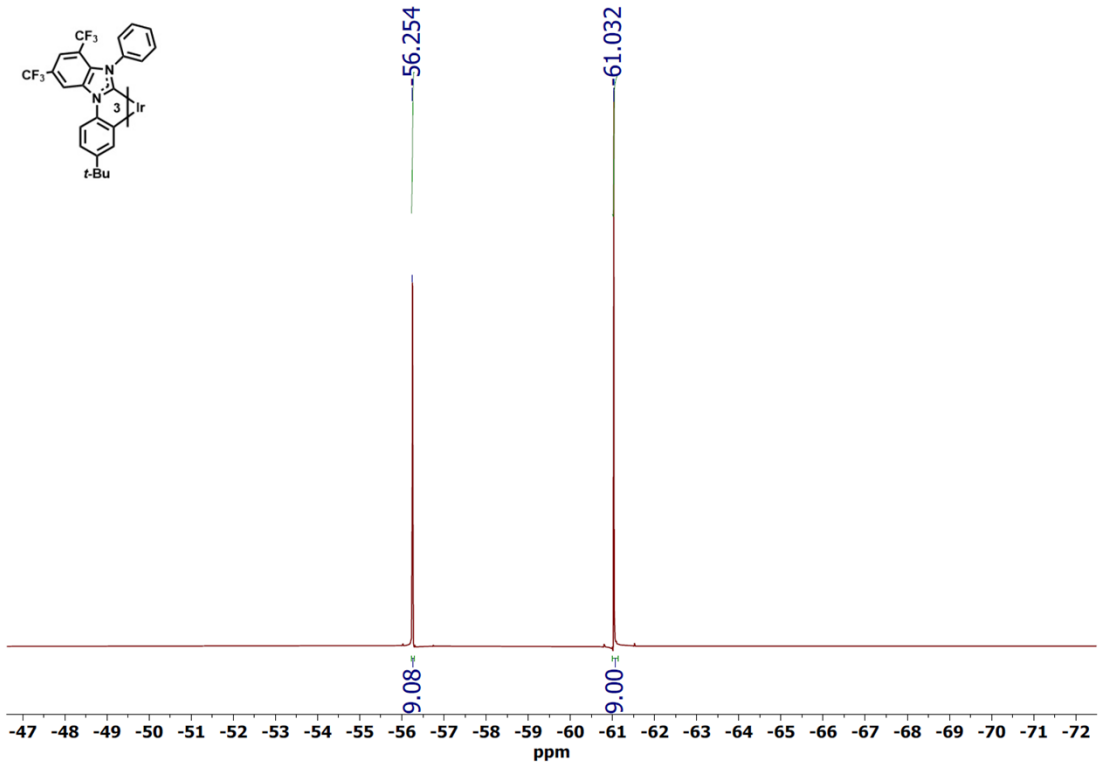

Figure S15. ^{19}F NMR (376 MHz) spectrum of ***f*-Ir(tBpp)$_3$** recorded in $CDCl_3$ solution at RT.

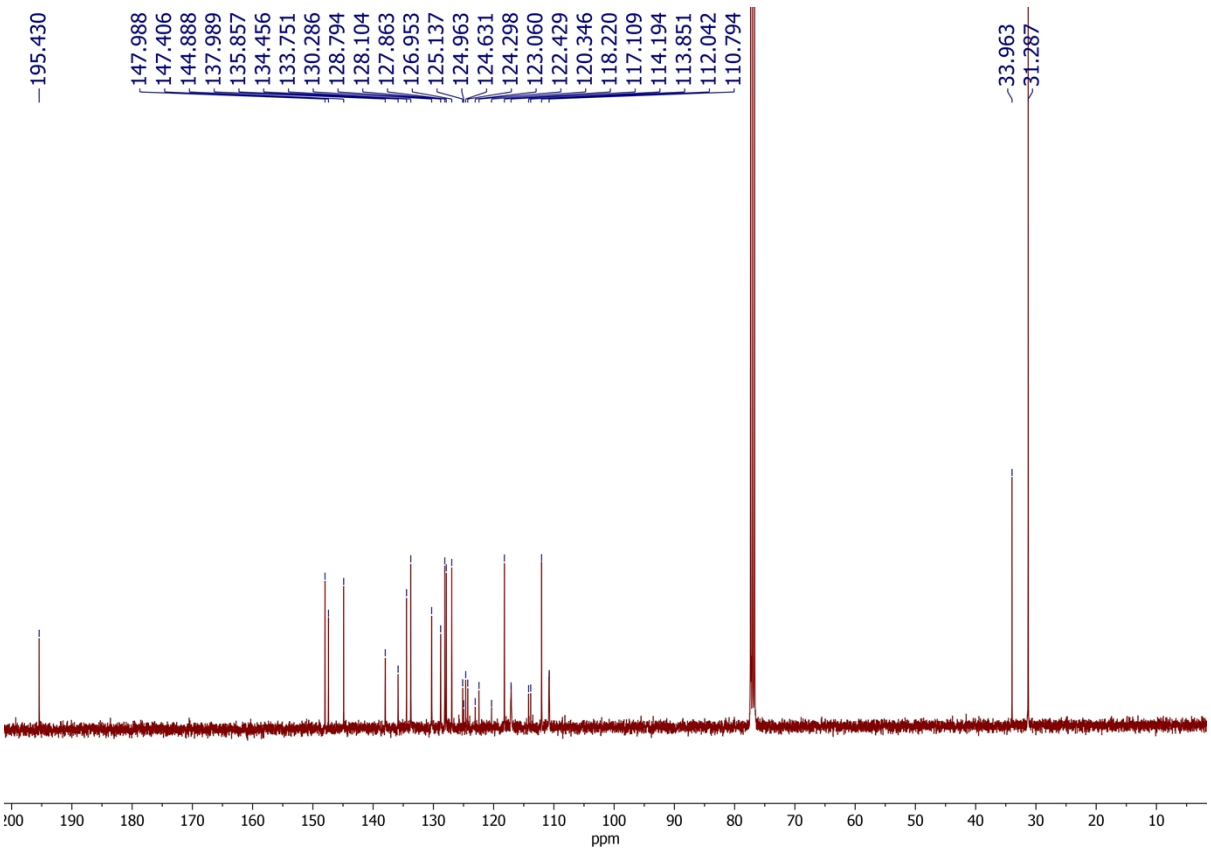

Figure S16. ^{13}C NMR (100 MHz) spectrum of ***f*-Ir(tBpp)$_3$** recorded in $CDCl_3$ solution at RT.

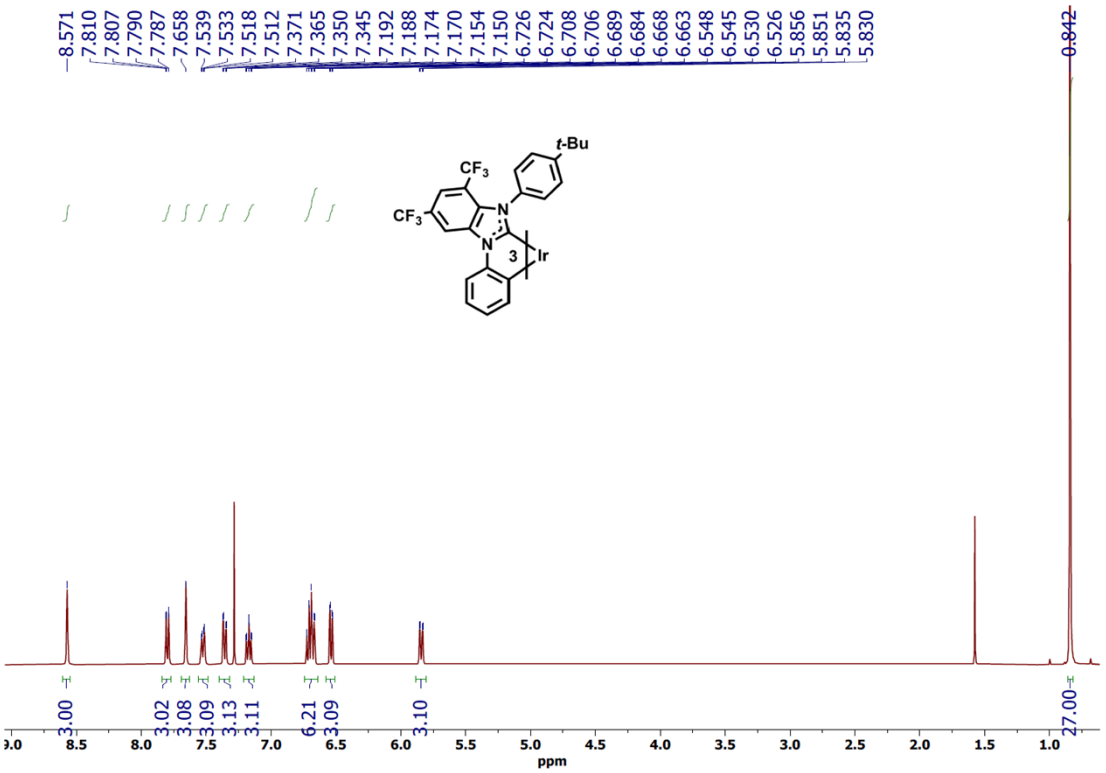

Figure S17. ^{1}H NMR (400 MHz) spectrum of ***f*-Ir(ptBp)$_3$** recorded in $CDCl_3$ solution at RT.

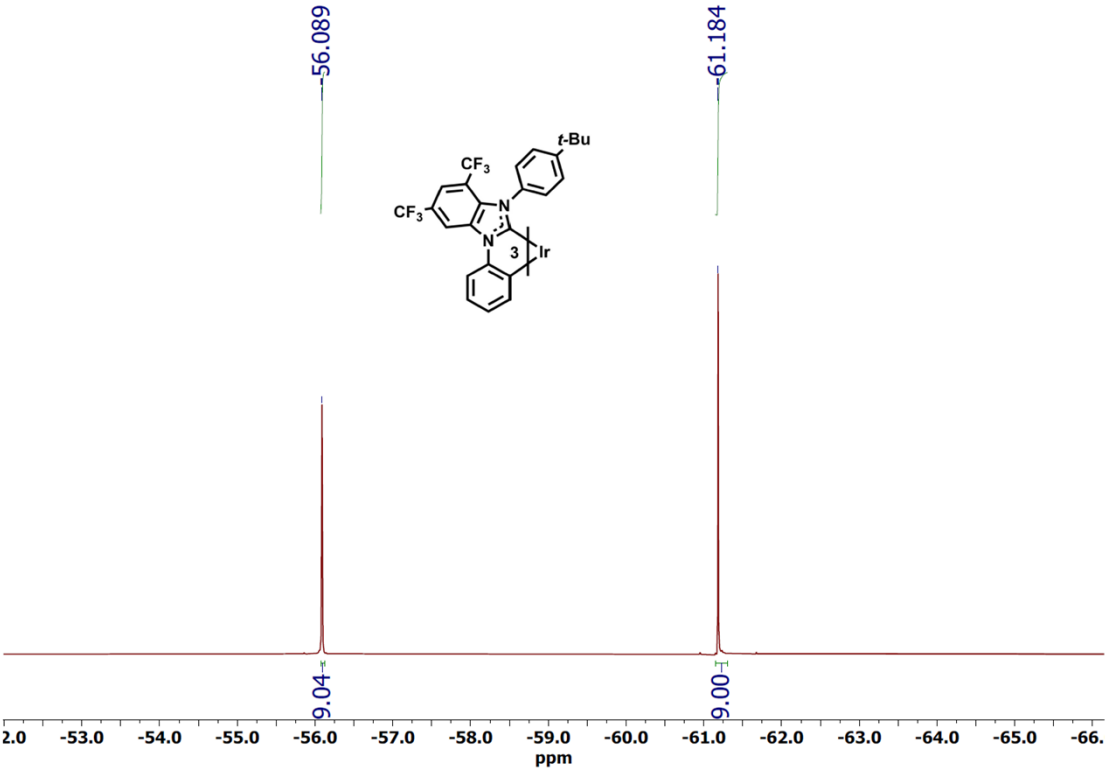

Figure S18. ^{19}F NMR (376 MHz) spectrum of ***f*-Ir(ptBp)$_3$** recorded in $CDCl_3$ solution at RT.

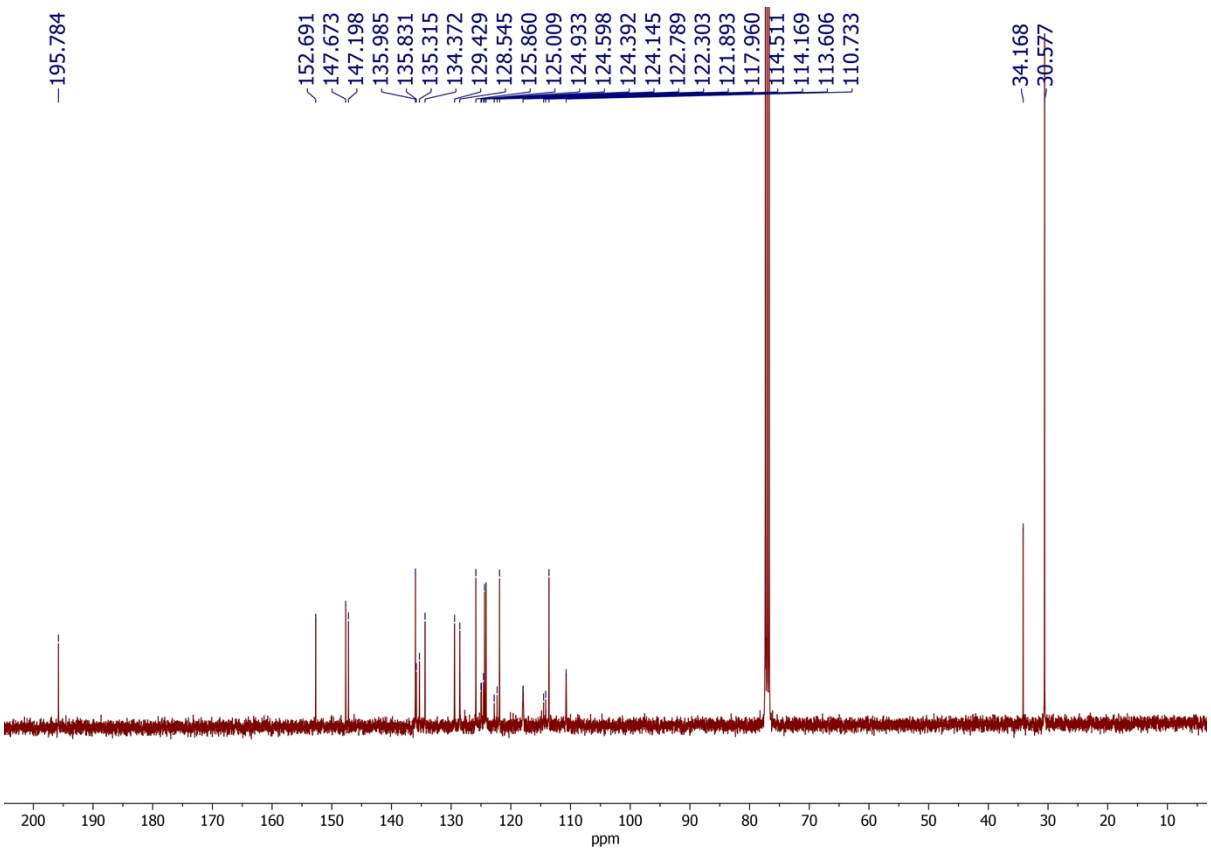

Figure S19. ^{13}C NMR (100 MHz) spectrum of ***f*-Ir(ptBp)$_3$** recorded in $CDCl_3$ solution at RT.

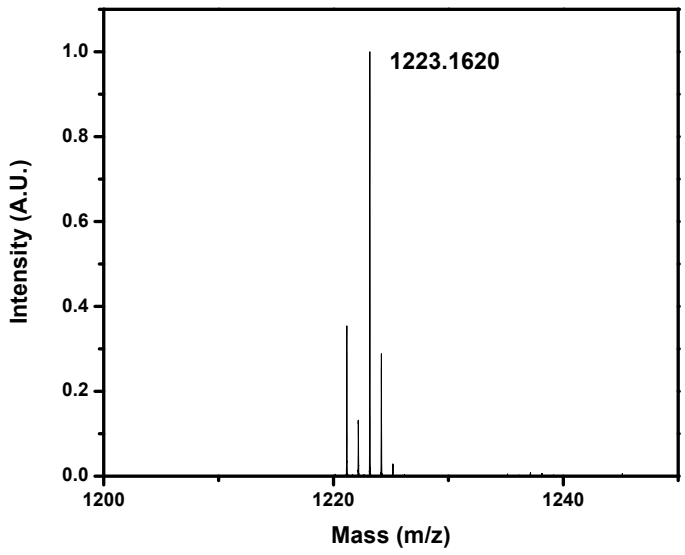

Figure S20. HRMS spectrum of ***m*-Ir(dfp)$_3$**.

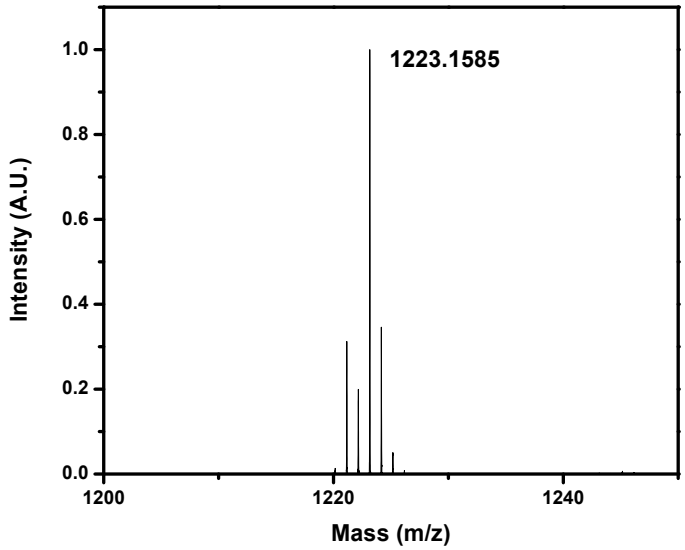

Figure S21. HRMS spectrum of ***f*-Ir(dfp)$_3$**.

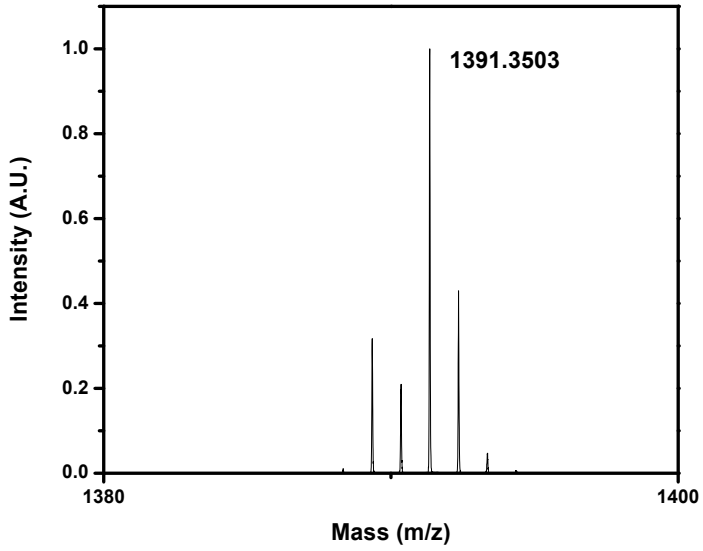

Figure S22. HRMS spectrum of ***f*-Ir(dfpb)$_3$**.

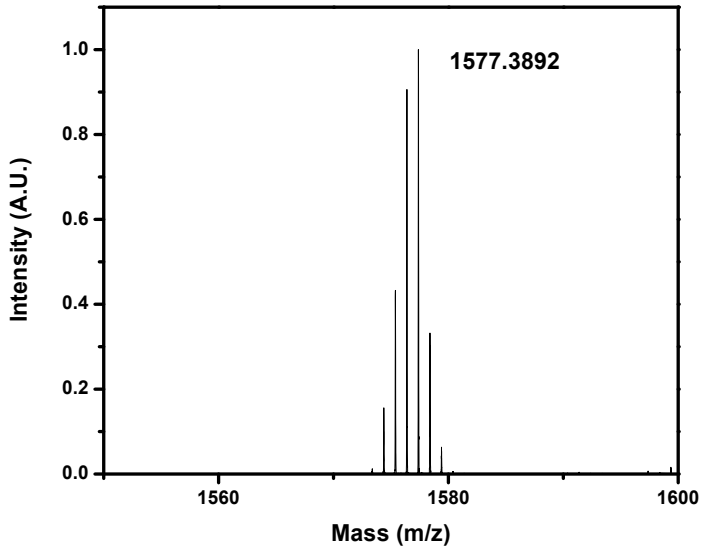

Figure S23. HRMS spectrum of ***f*-Ir(tBpp)$_3$**.

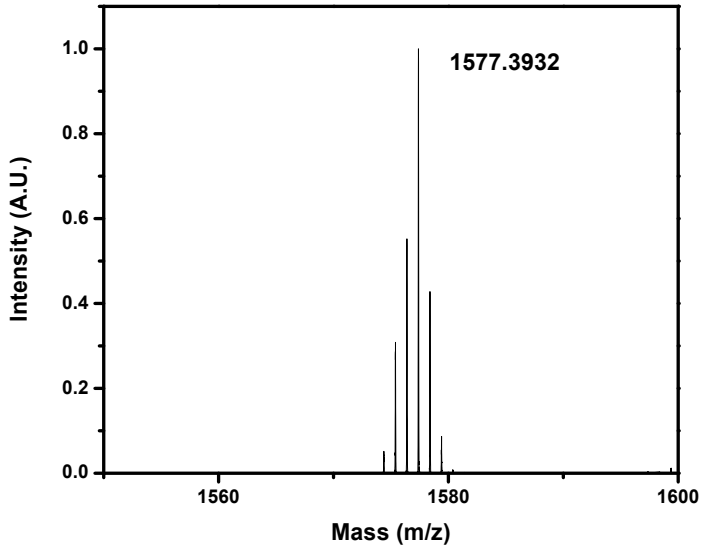

Figure S24. HRMS spectrum of ***f*-Ir(dfpb)$_3$**.

References

1. (a) C. Lee, W. Yang and R. G. Parr, *Phys. Rev. B*, 1988, **37**, 785-789; (b) A. D. Becke, *J. Chem. Phys.*, 1993, **98**, 5648-5652; (c) F. Weigend and R. Ahlrichs, *Phys. Chem. Chem. Phys.*, 2005, **7**, 3297-3305; (d) F. Weigend, *Phys. Chem. Chem. Phys.*, 2006, **8**, 1057-1065; (e) S. Grimme, S. Ehrlich and L. Goerigk, *J. Comput. Chem.*, 2011, **32**, 1456-1465.
2. M. J. Frisch, G. W. Trucks, H. B. Schlegel, G. E. Scuseria, M. A. Robb, J. R. Cheeseman, G. Scalmani, V. Barone, B. Mennucci, G. A. Petersson, H. Nakatsuji, M. Caricato, X. Li, H. P. Hratchian, A. F. Izmaylov, J. Bloino, G. Zheng, J. L. Sonnenberg, M. Hada, M. Ehara, K. Toyota, R. Fukuda, J. Hasegawa, M. Ishida, T. Nakajima, Y. Honda, O. Kitao, H. Nakai, T. Vreven, J. A. Montgomery, J. E. Peralta, F. Ogliaro, M. Bearpark, J. J. Heyd, E. Brothers, K. N. Kudin, V. N. Staroverov, R. Kobayashi, J. Normand, K. Raghavachari, A. Rendell, J. C. Burant, S. S. Iyengar, J. Tomasi, M. Cossi, N. Rega, J. M. Millam, M. Klene, J. E. Knox, J. B. Cross, V. Bakken, C. Adamo, J. Jaramillo, R. Gomperts, R. E. Stratmann, O. Yazyev, A. J. Austin, R. Cammi, C. Pomelli, J. W. Ochterski, R. L. Martin, K. Morokuma, V. G. Zakrzewski, G. A. Voth, P. Salvador, J. J. Dannenberg, S. Dapprich, A. D. Daniels, Ö. Farkas, J. B. Foresman, J. V. Ortiz, J. Cioslowski and D. J. Fox, *Gaussian 16, Revision C.01; Gaussian Inc.*, 2016, Wallingford, CT.
3. (a) S. Miertuš, E. Scrocco and J. Tomasi, *Chem. Phys.*, 1981, **55**, 117-129; (b) S. Miertuš and J. Tomasi, *Chem. Phys.*, 1982, **65**, 239-245.
4. (a) C. Adamo and D. Jacquemin, *Chem. Soc. Rev.*, 2013, **42**, 845-856; (b) A. D. Laurent, C. Adamo and D. Jacquemin, *Phys. Chem. Chem. Phys.*, 2014, **16**, 14334-14356.
5. R. L. Martin, *J. Chem. Phys.*, 2003, **118**, 4775-4777.
6. T. Lu and F. Chen, *J. Comput. Chem.*, 2012, **33**, 580-592.
7. F. L. Hirshfeld, *Theo. Chim. Acta*, 1977, **44**, 129-138.
8. B. de Souza, G. Farias, F. Neese and R. Izsák, *J. Chem. Theory Comput.*, 2019, **15**, 1896-1904.
9. (a) E. van Lenthe, E. J. Baerends and J. G. Snijders, *J. Chem. Phys.*, 1993, **99**, 4597-4610; (b) E. van Lenthe, E. J. Baerends and J. G. Snijders, *J. Chem. Phys.*, 1994, **101**, 9783-9792.
10. F. Neese, F. Wennmohs, U. Becker and C. Riplinger, *J. Chem. Phys.*, 2020, **152**, 224108.
11. C. C. Pye and T. Ziegler, *Theor. Chem. Acc.*, 1999, **101**, 396-408.